604–612 Nucleic Acids Research, 1994, Vol. 22, No. 4 © 1994 Oxford University Press

# Structural characterization of a ribonuclease III processing signal

David C.Schweisguth, Bhadrani S.Chelladurai[1], Allen W.Nicholson[1,*] and Peter B.Moore
Departments of Chemistry and Molecular Biophysics and Biochemistry, Yale University, PO Box 6666, New Haven, CT 06511-8118 and [1]Department of Biological Sciences, Wayne State University, Detroit, MI 48202, USA

Received November 10, 1993; Revised and Accepted January 13, 1994

## ABSTRACT

**The structure of a ribonuclease III processing signal from bacteriophage T7 was examined by NMR spectroscopy, optical melting, and chemical and enzymatic modification. A 41 nucleotide variant of the T7 R1.1 processing signal has two Watson – Crick base-paired helices separated by an internal loop, consistent with its predicted secondary structure. The internal loop is neither rigidly structured nor completely exposed to solvent, and seems to be helical. The secondary structure of R1.1 RNA is largely insensitive to the monovalent cation concentration, which suggests that the monovalent cation sensitivity of secondary site cleavage by RNase III is not due to a low salt-induced RNA conformational change. However, spectroscopic data show that $Mg^{2+}$ affects the conformation of the internal loop, suggesting a divalent cation binding site(s) within this region. The $Mg^{2+}$-dependence of RNase III processing of some substrates may reflect not only a requirement for a divalent cation as a catalytic cofactor, but also a requirement for a local RNA conformation which is divalent cation-stabilized.**

## INTRODUCTION

Protein recognition of double-stranded RNA is important in many gene regulatory mechanisms [1–3]. *Escherichia coli* ribonuclease III (RNase III, E.C.3.1.24)[1] [4] is an endonuclease that specifically hydrolyzes dsRNA (reviewed in [5]). It cleaves primary rRNA transcripts, releasing the immediate precursors to the 16S and 23S rRNAs. A number of cellular pre-mRNAs are also substrates for RNase III. RNA cleavage occurs at specific sites called RNase III processing signals, which invariably contain approximately two turns of more or less regular dsRNA. Additional sequence and structural elements are present in RNase III processing signals which determine the way they are cleaved, and often have important functional consequences for the metabolic stabilities and translational activities of the transcripts [5].

The life cycles of a number of coliphages depend on RNase III. The early region of the bacteriophage T7 genome, for example, encodes five RNase III processing signals that occur in the intercistronic regions, and several cleavage sites have been found in transcripts from the T7 late region [6]. RNase III cleavage of the early primary transcript creates mature mono- and dicistronic mRNAs, and also determines their translational activities and stabilities [6–8]. The T7 R1.1 processing signal (Figure 1), immediately upstream of gene 1.1, is an approximately 60 nt, irregular RNA hairpin, consisting of two dsRNA segments which are separated by an asymmetric internal loop. It contains the sequence information which is necessary and sufficient for accurate *in vitro* RNase III cleavage [9,10]. The R1.1 element is cleaved at a single point within the internal loop, leaving a short hairpin which protects the upstream RNA segment from 3′–5′ exonucleolytic degradation [6,11]. The R1.1 processing signal has been placed in plasmid expression vectors in order to produce transcripts with precisely defined 5′ ends, or having prolonged metabolic stabilities [12–14].

Although over 30 different RNase III processing signals have been identified, and several studied biochemically and genetically, little is known about their solution conformations. The T7 R1.1 RNA has been studied as a model substrate with which to determine the RNA sequence and structural elements that establish RNase III processing reactivity [10,15]. Determination of its structure may provide information as to why some substrates are cleaved once, while others undergo coordinate double cleavage, and afford insight into the reason for secondary site cleavage and its dependence on salt concentration. In this report we describe imino proton NMR and optical melting studies of the R1.1 processing signal, and the results of enzymatic and chemical probing experiments using reagents specific for structured or unstructured RNA regions. The data indicate that the R1.1 processing signal is extensively base-paired, and that its internal loop is helical in character but is less stable than a canonical dsRNA element. The conformation of the R1.1 processing signal is largely insensitive to the monovalent salt concentration, suggesting that the influence of salt on secondary site cleavage by RNase III reflects altered interactions between

*To whom correspondence should be addressed

enzyme and substrate rather than changes in RNA structure. In contrast, $Mg^{2+}$ does influence the conformation of the internal loop. Divalent cations may direct the pattern RNase III processing by altering substrate structure, as well as serving as essential catalytic cofactors.

## MATERIALS AND METHODS

### Materials

Water was deionized and distilled. Chemicals were reagent grade. Ribonucleoside triphosphates were purchased from Boehringer-Mannheim. [$\gamma$-$^{32}$P]ATP (3000 Ci/mmol) and [$\alpha$-$^{32}$P]UTP (3000 Ci/mmol) were purchased from Dupont-NEN. DEPC and DMS were obtained from Aldrich, while RNases U2, T2, and T1 were from GIBCO-BRL, and RNase V1 from Pharmacia. T7 RNA polymerase and RNase III were purified as described from overexpressing bacterial strains [16,17]. The oligodeoxynucleotide transcription templates were synthesized at the Wayne State Macromolecular Analysis Facility, and the fully deprotected forms purified by denaturing gel electrophoresis [10]. The sequence of the R1.1[LSΔ6] RNA template, and the 18 nt promoter oligonucleotide are as follows: 5′-AGGATCATAAA-GGCCACTCTTGCGAATGACCTTGAGTTCCCTATAGTG-AGTCGTATTA-3′; 5′-TAATACGACTCACTATAG-3′.

### RNA synthesis and purification

Preparative-scale synthesis of R1.1[LSΔ6] RNA was carried out by the procedure of Uhlenbeck and coworkers [18] with the modifications described by Wyatt *et al.* [19]. Transcription reactions (5−10 ml) were prepared in standard buffer [18], which included 4 mM of each ribonucleoside triphosphate, 20 mM $Mg^{2+}$, T7 RNA polymerase (2500 units/ml) and 55 nM of transcription template annealed to the promoter oligonucleotide. Following incubation for 4 hours at 37°C, the reactions were terminated by adding EDTA (50 mM final concentration), dialyzed against water, then phenol extracted and ethanol precipitated. The crude RNA was resuspended in water and electrophoresed (25 V/cm) in 1.5 mm thick, 15% polyacrylamide gels containing 7 M urea in TBE buffer. The gel region containing the full-length transcript was located by UV-shadowing. Minor amounts of longer RNA species were also observed, representing transcripts with one or two additional nucleotides at the 3′ terminus [18]. The RNA was extracted from crushed gel bands using 0.5 M ammonium acetate, 1 mM EDTA (pH 7). The aqueous volume was reduced by repeated extraction with 1-butanol, and the RNA ethanol-precipitated and resuspended in $H_2O$. The yield was determined by UV absorbance (calculated extinction coefficient: $4.45\times10^5$ $M^{-1}$ $cm^{-1}$). 5′-$^{32}$P-labeled R1.1[LSΔ6] RNA was prepared by dephosphorylation of unlabeled transcript with calf alkaline phosphatase, followed by reaction (approximately 50 pmol; 30 minutes at 37°C) with T4 polynucleotide kinase (20 units) and [$\gamma$-$^{32}$P] ATP (0.89 $\mu$M; 1870 Ci/mmol) in kinase buffer. The $^{32}$P-labeled RNA was purified by gel electrophoresis as described above. Base-specific cleavage analysis of $^{32}$P-labeled R1.1[LSΔ6] RNA using RNases T1 and U2 was in full agreement with the predicted sequence.

### NMR spectroscopy

All NMR experiments were conducted on a sample containing approximately 0.6 $\mu$mol of R1.1[LSΔ6] RNA. Buffers contained 4 mM sodium cacodylate and 0.2 mM EDTA, pH 7.5, with 200 mM KCl and/or 5 mM $MgCl_2$ added as described. The RNA was dialyzed extensively against each of the buffers in which it was to be examined and concentrated to approximately 400 $\mu$l in a Centricon-3 concentration device (Amicon). 20 $\mu$l $D_2O$ (MSD Isotopes) was added to the sample as a lock reference and 1 $\mu$l 2.5% dioxane as a chemical shift standard. The chemical shift of dioxane was taken to be 3.741 ppm at all temperatures.

One-dimensional spectra were water-suppressed using the twin-pulse method [20]. Difference NOE experiments were collected in interleaved sets of 64 scans, irradiating each frequency of interest in turn with a 300 ms low-power pulse [21]. Two-dimensional NOESY spectra were collected in phase-sensitive mode with States phase cycling and a 300 ms mixing time. Water was suppressed using a self-refocused 1331 pulse before acquisition [22]. 2048 complex points were collected in t2 and approximately 300 points were collected in t1. All data were apodized with 30° to 70°-shifted sine bells before Fourier transformation.

One-dimensional NMR experiments were done using a homebuilt 490 MHz spectrometer and NOESYs were collected on a Bruker AM-500, both in Yale's Chemical Instrumentation Center. Data were processed on a Silicon Graphics workstation using Felix (Hare Research).

### Optical melting

Aliquots of R1.1[LSΔ6] RNA were dialyzed extensively against each buffer, diluted to concentrations of 0.1, 0.3, 1, 3 and 10 OD, degassed under vacuum, and placed in stoppered quartz cuvettes with path lengths of 1 cm (0.1, 0.3 and 1 OD samples) or 0.1 cm (3 and 10 OD samples). Melting was done in a Varian Cary 1 UV-visible double-beam spectrophotometer. Five samples, one at each concentration, were melted simultaneously. Cuvettes filled with degassed buffer were used as references. The temperature was raised from 5 to 95 °C at 0.5 °C per minute and the absorbance at 260 nm of each sample recorded every 0.5 °C. The temperature was returned to 20 °C at the end of each melt and the absorbance checked to ensure that solvent had not been lost by evaporation during the melt. Each melt was done in duplicate.

Melting data were normalized to 1 OD at 20 °C and duplicates were averaged. Observed absorbance was modeled as the sum of a baseline (the absorbance of fully stacked RNA) and two sigmoids (the hypochromicities of two independently melting regions), each varying linearly with temperature, using the following equation:

$$A = a_0 + b_0 T + \frac{a_1 + b_1 T}{1 + e^{\frac{\Delta H^\circ_1}{R}\left(\frac{1}{T} - \frac{1}{T_{m,1}}\right)}} + \frac{a_2 + b_2 T}{1 + e^{\frac{\Delta H^\circ_2}{R}\left(\frac{1}{T} - \frac{1}{T_{m,2}}\right)}}$$

A is absorbance, T is temperature, $\Delta H^\circ_1$ and $\Delta H^\circ_2$ are the enthalpies of the two transitions, $T_{m1}$ and $T_{m2}$ are their melting temperatures and $a_n$ and $b_n$ are the zero and first-order coefficients of variation of each term with temperature. This equation was fit to the averaged data using an implementation of the simplex algorithm [23]. Nearly all fits converged to the data within a RMS difference of $10^{-6}$; those which did not, due to experimental error, were rejected. Restarting converged fits did not significantly change either the values of the parameters or the goodness of fit. The enthalpies and $T_m$ values were averaged, and the standard deviations calculated. Entropies were

calculated as $\Delta H°/T_m$ and free energies at 37 °C as $\Delta H° - (310.15\,K \cdot \Delta S°)$. Enthalpies, entropies and energies for the upper and lower stems were summed to obtain the parameters for the entire molecule.

### Enzymatic and chemical structure probing

The protocols followed for probing of 5′-$^{32}$P-labeled R1.1[LSΔ6] RNA using RNase T2 or RNase V1 were based on those described previously [24]. Chemical probing using DMS or DEPC was carried out essentially as described elsewhere [25]. The reaction buffer was 4 mM sodium cacodylate (pH 7.5), 0.2 mM EDTA, supplemented with 200 mM KCl and/or 5 mM $MgCl_2$, as indicated. Enzymatic RNA sequencing reactions were performed using RNase U2 or RNase T1, following the protocol provided by GIBCO-BRL. Reactions were analyzed by electrophoresis in 0.4 mm thick, 15% polyacrylamide, 1.5% bisacrylamide sequencing gels containing 7 M urea and TBE buffer. Autoradiography was carried out using Fuji RX film and intensifying screens.

## RESULTS

### Choice of experimental target

R1.1[LSΔ6] RNA , shown in Figure 1B, is a 41-nt derivative of the T7 R1.1 processing signal. The RNA incorporates the wild-type upper stem and asymmetric internal loop, and possesses a lower stem of sufficient size for the RNA to be faithfully processed by RNase III *in vitro*, albeit with a reduced reactivity compared with the wild type sequence [15]. Unlike its parent molecule, R1.1[LSΔ6] RNA has helices of different lengths, avoiding ambiguity in assigning the results of NMR spectroscopy and optical melting to the correct parts of the molecule. Its lower stem lacks 5′ or 3′ single-stranded extensions, reducing the likelihood of intermolecular aggregation [26].

The RNase III reactivity of R1.1[LSΔ6] RNA was tested in the buffer used in the NMR experiments (4 mM cacodylate, 5 mM $Mg^{2+}$, 200 mM KCl). The RNA was cleaved singly at the canonical site, at a rate comparable to that observed in the physiologically relevant potassium glutamate-based buffer [17] (data not shown). Moreover, when KCl as omitted from the reaction buffer cleavage occurred at the expected secondary site (data not shown). We conclude that the cacodylate-based buffer does not perturb R1.1[LSΔ6] RNA structure in a manner that inhibits the proper pattern of primary and secondary site enzymatic processing.

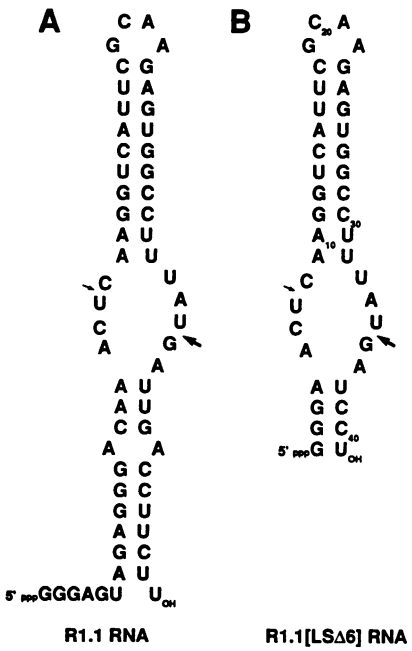


**Figure 1.** Sequence and secondary structure of (**A**) the T7 R1.1 processing signal and (**B**) R1.1[LSΔ6] RNA.

### Spectroscopic analysis

Downfield spectra of R1.1[LSΔ6] RNA at 5 °C in three different ionic conditions are shown in Figure 2. Each spectrum shows thirteen peaks of roughly stoichiometric intensity, representing G or U imino protons protected from solvent by hydrogen-bonding, and six to ten peaks of lesser intensity, representing imino protons in faster exchange with solvent or with each other. Thus, all or nearly all of the 22 imino protons in R1.1[LSΔ6] RNA are visible and are at least somewhat protected from solvent exchange at 5 °C in each ionic condition. There are also several low-intensity but narrow peaks, due either to minor conformations or small amounts (less than 1%) of transcripts with 3′ extensions (see Materials and Methods). The chemical shifts of the stoichiometric resonances change relatively little with ionic conditions. Most of the differences between these spectra reflect changes in the weaker resonances.

Spectra collected at temperatures up to 60 °C, or 30 °C when the solvent contained $Mg^{2+}$ (data not shown), demonstrated that although the imino proton exchange rates increase with temperature, no resonances disappear (except through increased exchange with solvent) and no new ones appear. Moreover, since the chemical shifts change only slightly, the RNA undergoes no

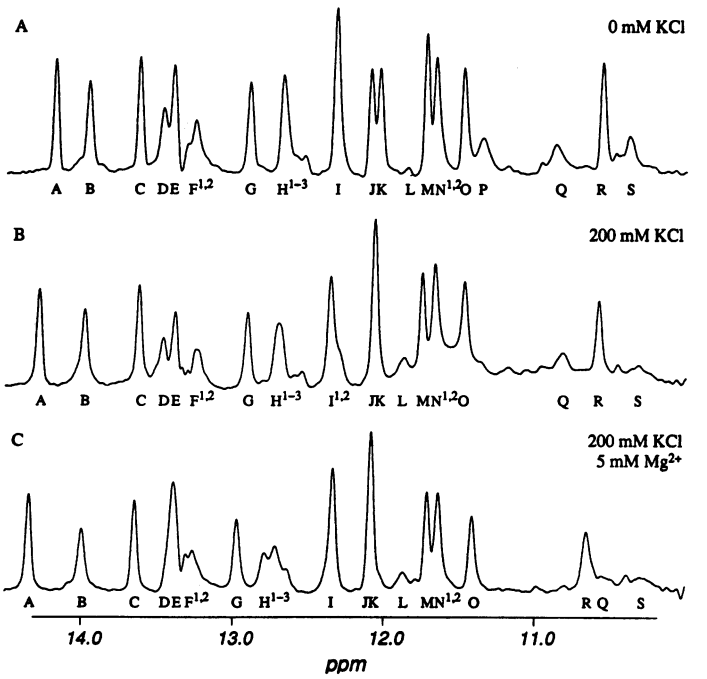


**Figure 2.** The imino region of the proton spectrum of R1.1[LSΔ6] RNA at 5 °C, collected as described in Materials and Methods. **A**, 0 mM KCl. **B**, 200 mM KCl. **C**, 200 mM KCl and 5 mM $MgCl_2$.

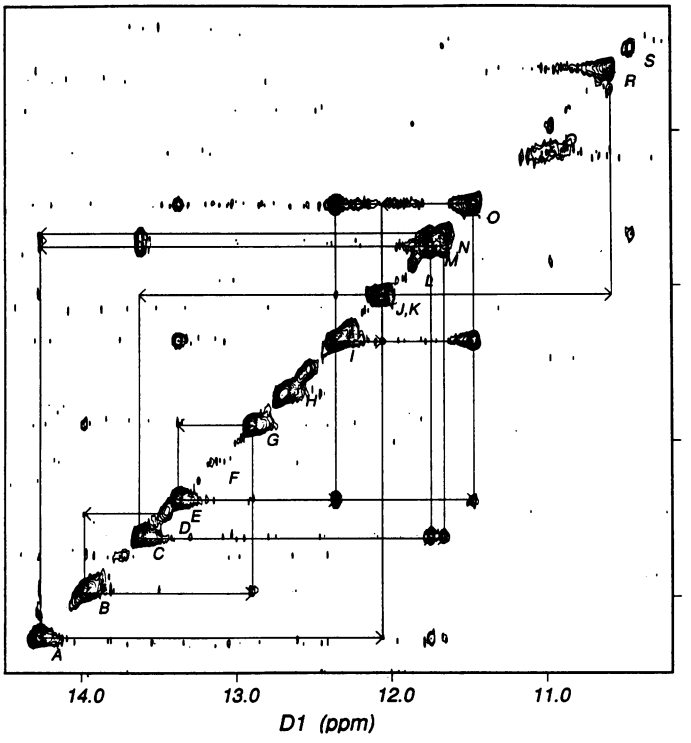


**Figure 3.** The imino–imino region of a proton–proton NOESY of R1.1[LSΔ6] RNA in 200 mM KCl at 5 °C, collected as described in Materials and Methods.

gross structural rearrangements as a function of temperature. This result was obtained under all ionic conditions tested.

The imino–imino region of a NOESY of R1.1[LSΔ6] RNA in 200 mM KCl at 5 °C is shown in Figure 3. Nearly all of the stoichometric resonances and some of the weak resonances correlate with one or two others, indicating spatial proximity. Sequences of adjacent imino resonances can thus be identified. NOESYs were also collected at 30 °C, where small changes in chemical shift at the higher temperature helped to resolve overlapping peaks (data not shown). One-dimensional difference NOE experiments (data not shown) were also carried out to confirm these results. Difference experiments were often more sensitive, but two-dimensional experiments provided higher resolution. Comparison between the two was important for confident assignment of NOEs.

The uracil imino proton in an A:U base pair typically shows a strong NOE to the adenine H2 proton. These NOEs were used to identify A:U pairs and align the sequence of adjacent imino protons determined by NOE experiments with that expected from the predicted secondary structure of R1.1[LSΔ6] RNA. The alignment is unambiguous in the upper stem-loop. All thirteen of the stoichiometric imino resonances originate in that part of the molecule. The assignments are summarized in Figure 4. It was not possible to distinguish between partners in the two G:U pairs in the upper stem by their NOEs, as each shows NOEs to its partner and to the imino protons in the base pairs above and below, as well as several NOEs to protons in the amino region. The guanine proton in a G:U pair is typically far upfield of the uracil proton, so peak O is probably a G and peak I a U, but peaks M and N cannot be thus assigned. Each resonance assigned to a uracil imino proton in an A:U base pair shows the expected U imino-AH2 NOE (data not shown). These

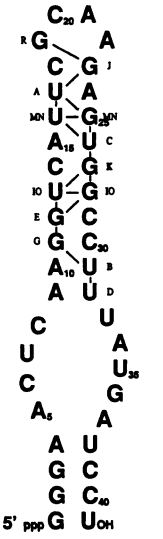


**Figure 4.** Assignments of imino resonances to R1.1[LSΔ6] RNA protons. Lines represent NOEs observed between imino protons. The assigned protons and the NOEs between them are present in each of the conditions examined, excepting the NOEs between K and I, G and B and B and D, which are weak or absent at 0 mM KCl, and that between R and J, which is absent in 5 mM $Mg^{2+}$.

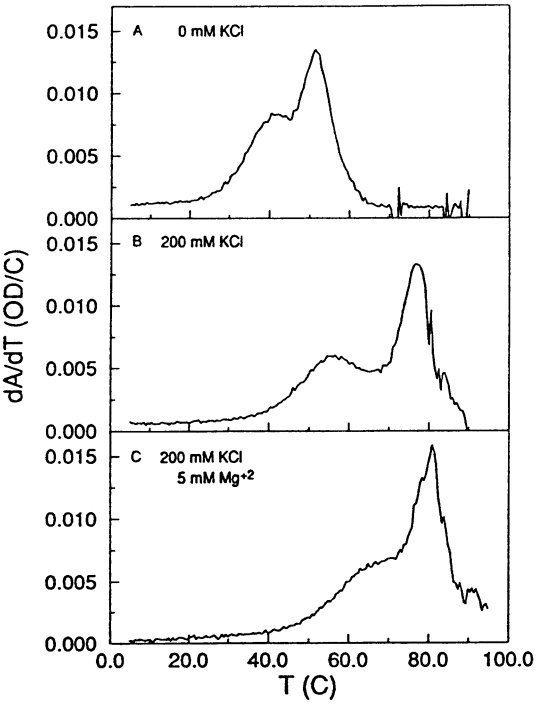


**Figure 5.** Absorbance at 260 nm of R1.1[LSΔ6] RNA (approximately 2.5 μM) as a function of temperature, differentiated with respect to temperature in order to highlight melting transitions. **A**, 0 mM KCl. **B**, 200 mM KCl. **C**, 200 mM KCl and 5 mM $MgCl_2$.

assignments are supported by data obtained from a related R1.1 RNA derivative having the same upper stem, but with a lower stem containing seven different Watson–Crick base pairs. All of the assigned protons are present in the spectrum of this R1.1 variant, and exhibit the same NOEs (data not shown).

**Table 1.** Thermodynamic parameters of R1.1[LSΔ6] RNA melting in the indicated solvents

| | Solvent | $T_m$ (°C) | ΔH° (kcal/mol) | ΔS° (cal/mol K) | $\Delta G°_{37}$ (kcal/mol) |
|---|---|---|---|---|---|
| **Lower stem** | 0 mM KCl | 39.4 ± 6.5 | 48.3 ± 0.7 | 154 ± 2 | 0.5 ± 1.0 |
| | 200 mM KCl | 55.1 ± 3.9 | 33.7 ± 2.3 | 103 ± 7 | 1.8 ± 3.2 |
| | 200 mM KCl + 5 mM $MgCl_2$ | 69.1 ± 0.2 | 29.6 ± 1.5 | 87 ± 4 | 2.0 ± 2.0 |
| **Upper stem** | 0 mM KCl | 51.4 ± 0.6 | 70.9 ± 5.8 | 218 ± 18 | 3.3 ± 8.0 |
| | 200 mM KCl | 76.5 ± 0.6 | 104.3 ± 14.7 | 298 ± 42 | 11.9 ± 19.7 |
| | 200 mM KCl + 5 mM $MgCl_2$ | 80.4 ± 0.4 | 125.3 ± 6.5 | 317 ± 16 | 27.0 ± 6.5 |
| **Total** | 0 mM KCl | | 119.2 ± 5.8 | 372 ± 17 | 3.8 ± 8.1 |
| | 200 mM KCl | | 138.0 ± 14.9 | 401 ± 43 | 13.7 ± 20.0 |
| | 200 mM KCl + 5mM $MgCl_2$ | | 154.9 ± 6.6 | 404 ± 17 | 29.0 ± 6.8 |

Parameters were calculated as described in Materials and Methods. Errors are standard deviations.

Peak R is assigned to the imino proton of $G_{19}$ in the tetraloop, which is expected to be protected from solvent exchange as discussed below. Two pairs of resonances, L and Q and $N_2$ and S, show detectable NOEs to each other but to no other protons. (The N and $N_2$ peaks overlap completely, but are distinguishable by the chemical shifts of their crosspeaks to other resonances in 0 mM KCl.) They are all broadened and shifted upfield by exchange, and thus most likely located in the loop or lower stem. The imino spectrum of the R1.1 variant mentioned above, in which the lower stem sequence is different, lacks the L and Q resonances, and the L-Q and $N_2$-S NOEs are not seen (data not shown). One of these pairs might arise from the G:U pair at the base of the lower stem. This would account for their strong mutual NOE, which is detectable despite the broadening of the individual resonances, and the absence of that NOE in the variant molecule, which does not have a G:U pair in the lower stem.

Similar experiments in buffers lacking $K^+$ or containing only 5 mM $Mg^{2+}$ gave similar results. Base-pairing in the upper stem is insensitive to $Mg^{2+}$ or the monovalent cation concentration, except the base pair represented by the unassigned resonance P, which is evident only in low salt, and the $A_9$:$U_{32}$ pair (peak D) adjacent to the internal loop, whose imino proton resonance shifts upon the addition of $Mg^{2+}$.

We conclude that the upper stem-loop of the R1.1 processing signal is stable in all solvent conditions tested. Of the six to ten unassigned resonances, no more than five can come from the four base pairs (one a G:U) in the lower stem. This indicates that at least one of the four imino protons in the internal loop is weakly protected from solvent exchange. Monovalent salt significantly affects no more than one base-pairing interaction in either the internal loop or lower stem. The addition of $Mg^{2+}$ affects the chemical shift of several imino proton resonances in the internal loop and lower stem, but neither creates nor destroys structural features which protect imino protons from solvent exchange.

## Optical melting

Figure 5 shows the absorbance of R1.1[LSΔ6] RNA at 260 nm as a function of temperature in each buffer, differentiated with respect to temperature to highlight the melting transitions. Two transitions are evident in each case, presumably corresponding to the melting of the upper and lower stems. That the transitions are distinct indicates a discontinuity in stacking in the internal loop, and the absence of a third transition suggests that internucleotide interactions in the internal loop either contribute little to meltable hypochromicity, or melt in concert with the upper or lower stem.

Melts were done at concentrations of RNA from 0.1 to 10 OD (0.25 to 25 μM). Melting behavior was independent of concentration in each buffer, showing that R1.1[LSΔ6] RNA is monomeric over this concentration range, and therefore almost certainly monomeric at the concentration used in the NMR experiments, which was less than 100-fold larger than the highest concentration melted.

Table 1 presents the thermodynamic parameters derived from these melting experiments, calculated assuming the two transitions to be independent. The transition with the larger enthalpies and entropies of melting is assigned to the upper stem, on the assumption that the magnitude of these parameters should increase with the size of the base-paired region [27]. In support of this, the related R1.1 molecule (see above) has two melting transitions, each having a much higher $T_m$ than that for the transition which we attribute to the lower stem of R1.1[LSΔ6] RNA (data not shown).

The upper stem melts well above 37 °C in all conditions, but the lower stem is mostly dissociated at 37 °C in 0 mM KCl. Melting temperatures and free energies of melting are higher in the presence of potassium and magnesium, which counteract charge repulsion between backbone phosphates. Interestingly, the enthalpies and entropies of melting decrease with increasing ionic strength in the lower stem, but increase in the upper stem. This may indicate that the bases in the internal loop stack on the lower stem at low ionic strength, but stack on the upper stem at high ionic strength.

## Chemical and enzymatic structure probing

To further define conformational features of the R1.1 processing signal, chemical and enzymatic structure probing was performed on 5′ $^{32}$P-labeled R1.1[LSΔ6] RNA. To correlate the results with the NMR data, the structure probing experiments were carried out at 30 °C in the presence or absence of 200 mM KCl or 5 mM $MgCl_2$ in pH 7.5 cacodylate buffer. The enzymes were selected as complementary probes, as RNase T2 cleaves unstructured RNA regions [24], while RNase V1 catalyzes the hydrolysis of helical or double-helical RNA [28]. The chemical reactivity of R1.1[LSΔ6] RNA was examined using DMS and DEPC. DMS probes the steric accessibility and electronic environment of guanine N7 atoms [24,25], while DEPC examines

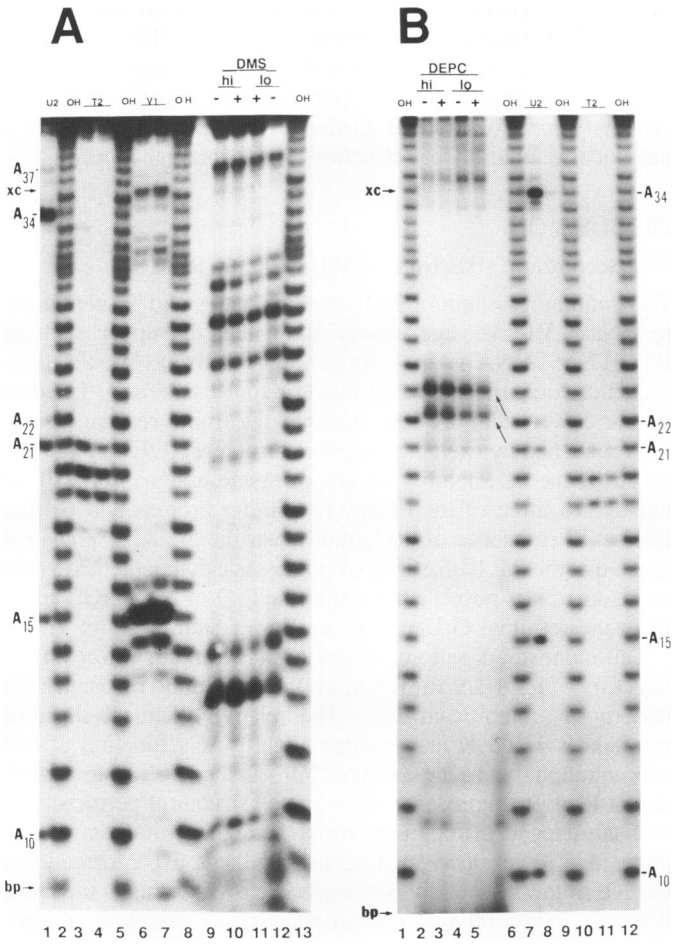


**Figure 6.** Chemical and enzymatic structure probing of R1.1[LSΔ6] RNA. Figure 7 summarizes the results. 5′-$^{32}$P-labeledR1.1[LSΔ6] RNA was prepared as described in Materials and Methods. For structure-probing with RNase T2 or RNase V1, $^{32}$P-labeled RNA ($6\times10^4$ dpm) was incubated with enzyme at 30 °C for 15 minutes in 10 μl of cacodylate buffer (pH 7.5) containing 200 mM KCl and 5 mM $MgCl_2$. Separate reactions (data not shown) omitted the KCl and/or $MgCl_2$. For DMS structure probing, $^{32}$P-labeled RNA ($3\times10^5$ dpm) was treated with 0.5 μl DMS for 15 minutes at 30 °C in cacodylate buffer (200 μl), with or without KCl and/or $MgCl_2$. For DEPC structure probing, $^{32}$P-labeled RNA ($3\times10^5$ dpm) was treated for 2 hours at 30 °C with 20 μl of DEPC in cacodylate buffer (200 μl), with or without KCl and/or $MgCl_2$. To generate the alkaline ladder, $^{32}$P-labeled RNA ($2\times10^5$ dpm ) in 10 μl of 0.25 M $NaCO_3$ buffer (pH 9.2) was heated at 90 °C for 7 minutes in a sealed glass capillary tube. The adenine ladder was generated by reacting $^{32}$P-labeled RNA ($6\times10^4$ dpm) with RNase U2 (1−2 units) at 55 °C for 15 minutes in 25 mM sodium citrate (pH 3.5), 7 M urea, 1 mM EDTA and 0.05% bromphenol blue and xylene cyanol dyes. Electrophoresis was performed as described in Materials and Methods. **A**. Lane 1: RNase U2 reaction (U2) ($1.2\times10^4$ dpm). Lanes 2,5,8,13: alkaline ladder (OH) ($2.3\times10^4$ dpm/lane). Lanes 3,4: RNase T2 (T2) (10 and 15 units, respectively; $10^4$ dpm/lane). Lanes 6,7: RNase V1 (V1) (0.02 and 0.04 units, respectively; $10^4$ dpm/lane). Lanes 9−12: DMS reactions ($1.9\times10^4$ dpm/lane). Lane 9, 200 mM KCl ('hi'), 0 mM $MgCl_2$ (−); lane 10, 200 mM KCl, 5 mM $MgCl_2$ (+); lane 11, 0 mM KCl ('lo') , 5 mM $MgCl_2$; lane 12, 0 mM KCl, 0 mM $MgCl_2$. **B**. Lanes 1,6,9,12: alkaline ladder; lanes 2−5, DEPC reactions ($4\times10^4$ dpm/lane); lane 2, 200 mM KCl; lane 3, 200 mM KCl, 5 mM $MgCl_2$; lane 4, 200 mM KCl, 0 mM $MgCl_2$; lane 5, 0 mM KCl, 0 M $MgCl_2$. Lanes 7,8: RNase U2 reactions (1 and 2 units, respectively). Lanes 10,11: RNase T2 reactions (10 and 15 units, respectively) in 200 mM KCl, 5 mM $MgCl_2$. The positions of the adenine residues are indicated. The DEPC and RNAse U2 cleavage reactions result in different 3′ terminal modifications, and the products therefore have different mobilities [24]; the two arrows between lanes 5 and 6 connect fragments with the same number of nucleotides. 'xc' and 'bp' refer to the positions of the xylene cyanol and bromphenol blue dye markers, respectively.

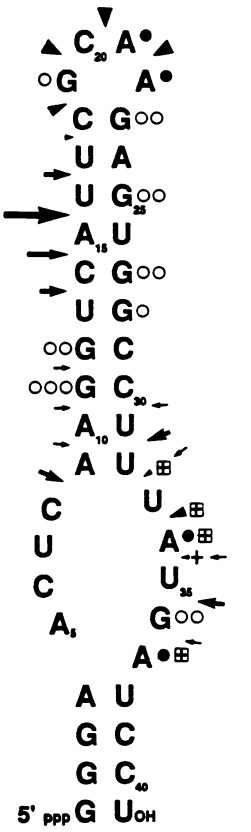


**Figure 7.** Summary of the enzymatically and chemically reactive sites in R1.1[LSΔ6] RNA. The solid circles indicate adenines susceptible to DEPC modification. Residues exhibiting increased reactivity in low salt are indicated with an enclosed '+' sign. The open circles denote guanines sensitive to DMS modification. The number of open circles reflect relative reactivities. The arrowheads indicate RNase T2 reactive phosphodiester bonds. The size of the arrowhead indicates relative reactivity, and those bonds whose reactivities increase in low salt are indicated by an arrowhead with an enclosed '+' sign. The arrows indicate sites of RNase V1 reactivity. The size of the arrow indicates relative cleavage reactivity.

adenine N7 atoms by the same criteria, with an additional difference being that DEPC cannot modify adenines in a regular double helix [24].

The results of representative experiments are shown in Figure 6 and summarized in Figure 7. At 200 mM KCl, essentially the only RNase T2-sensitive region in R1.1[LSΔ6] RNA is the GC-AA tetraloop ($G_{19}$,$C_{20}$,$A_{21}>C_{18}>U_{17}$) (Figure 6A, lanes 3 and 4; and Figure 6B, lanes 10 and 11). This result supports the spectroscopic evidence for base-paired upper and lower stems. A minor amount of RNase T2 cleavage occurs in the internal loop at the 3′ end-proximal side ($U_{33}>U_{32}$,$A_{34}$) (Figure 6A, lanes 3 and 4), suggesting some deviation from a stable structure in this region. Omitting KCl lowers the overall RNase T2 reactivity of the RNA, but increases the relative reactivity of the internal loop compared to the tetraloop (data not shown), suggesting that low salt destabilizes the internal loop structure (see also below). The presence of $Mg^{2+}$ has no effect on the RNase T2 reactivity pattern in high salt (data not shown), and omitting $Mg^{2+}$ in low salt buffer inhibits all RNase T2 cleavage. However, RNase T2 is able to cleave the top of the internal loop with low efficiency in low-salt with $Mg^{2+}$, and under the same

conditions RNase III is able to cleave a second time in the internal loop. If these differences in enzymatic reactivity result solely from monovalent ion-induced changes in RNA structure, those changes must be quite subtle and largely undetectable using these techniques.

As anticipated, R1.1[LSΔ6] RNA is sensitive to RNase V1, but the cleavage pattern is quite selective. In 200 mM KCl, 5 mM $MgCl_2$ the most reactive region is the 5′ side of the upper stem, with $A_{15}$ as the most reactive residue. A lesser amount of cleavage occurs at the flanking nucleotides $U_{13}$, $C_{14}$ and $U_{16}$ (Figure 6A, lanes 6 and 7). The reactivity of these sites is consistent with the double-helical nature of the upper stem. Some reactivity is also observed at several nucleotides centered at $A_{10}$, which is also located in the upper stem. Interestingly, the 3′ end-proximal segment of the internal loop is also cleaved by RNase V1. Specifically, a significant amount of cleavage occurs at $U_{35}$, which is also the primary RNase III cleavage site (Figure 6A, lanes 6 and 7). Additional cleavages are observed at flanking residues $A_{34}$ and $G_{36}$, as well as $C_{30}$, $U_{31}$ and $U_{32}$, indicating that this portion of the internal loop possesses (or has access to) a helical structure. There is no significant RNase V1 reactivity of the sequence between $A_{37}$ and the 3′ end (Figure 6A), or the sequence between the 5′ end and $U_8$ (data not shown). The lack of RNase V1 reactivity of these segments does not rule out the double-stranded nature of the lower stem, as nonuniform reactivities of dsRNA towards RNase V1 have been observed elsewhere [29,30], and reflect the specifics of RNase V1 interaction with helical RNA. Moreover, both of these segments are resistant to RNase T2 (see above), supporting the double-helical nature of this region. Finally, RNase V1 cleavage of R1.1[LSΔ6] RNA is greatly inhibited at low salt (data not shown), and omitting $Mg^{2+}$ abolishes all cleavage, reflecting the divalent cation requirement of RNase V1 [28].

The DMS reactivity pattern of R1.1[LSΔ6] RNA at 30°C in 200 mM KCl indicates that all guanine N7 atoms are reactive, with no guanine residue notably more reactive than the others (the methylation sensitivity of $G_1$, $G_2$ and $G_3$ could not be definitively assessed, due to the compressed gel electrophoretic mobilities of the short RNA products). Moreover, the DMS reactivity pattern is insensitive to KCl or $Mg^{2+}$ (Figure 6A, lanes 9−12). Specifically, we observe that the N7 of $G_{36}$ in the internal loop is no more reactive than the other guanine N7 atoms, indicating that $G_{36}$ is not looped out or otherwise solvent exposed. Interestingly, $G_{19}$ in the tetraloop is significantly less reactive than the other guanine residues, and the relative amount of DMS methylation of this residue does not increase at 90 °C (data not shown). The reduced reactivity may reflect the local electronic and steric environment of G19 within the highly structured context of the GCAA tetraloop [31,32]. The DEPC pattern indicates that $A_{21}$ and $A_{22}$ in the tetraloop are the most reactive residues (Figure 6B, lanes 2−5). A smaller yet significant amount of reaction is observed at $A_{34}$ and $A_{37}$ ($A_{34} > A_{37}$), whose DEPC sensitivities are enhanced in low salt. The low salt reactivity enhancement is not seen with the other adenines in the upper stem-loop. The DEPC sensitivities of $A_3$ and $A_4$ could not be definitively assessed, due to the small size of the reaction products and the differing mobilities of enzyme and DEPC-cleaved fragments (see also the legend to Figure 6). The overall DEPC reactivity pattern is insensitive to $Mg^{2+}$ in either the absence or presence of 200 mM KCl (Figure 6B, lanes 2−5). The lack of reactivity of the adenine residues in the upper stem is evidence for their existence within an A-form double helix [24]. Minor DEPC reactivity was observed with non-adenine residues in the tetraloop and internal loop. The DEPC sensitivity of non-adenine nucleotides in non-double-helical regions has been noted elsewhere [24]. This particular aspect of the DEPC reactivity pattern provides further evidence for the lack of a canonical double helical structure in the internal loop.

## DISCUSSION

### The secondary structure of R1.1[LSΔ6] RNA

The continuous chain of NOE connectivities and susceptibility to RNase V1 cleavage clearly show that the upper stem of R1.1[LSΔ6] RNA is an A form double helix, as predicted by sequence comparison (see [10] and references therein). The data for the lower stem are less clear, as the imino resonances are too broadened by exchange to give detectable NOEs. However, given (i) the detectability (if not complete assignability) of all but one to three of the twenty-two imino protons and (ii) the RNase T2 resistance of nucleotides near the 5′ and 3′ ends, we argue that the R1.1[LSΔ6] RNA possesses a double-helical lower stem. Also, it is possible that either the L-Q or $N_2$-S NOE arises from the terminal G:U pair in the lower stem.

The monovalent salt concentration has a minor effect on the structure of R1.1[LSΔ6] RNA, as only one imino resonance (P) undergoes a significant shift. The relative chemical shifts of resonances J and K also change slightly as a function of salt concentration, but as the chain of NOEs in the upper stem persists this is likely to represent only a minor structural perturbation. The salt-dependent, opposing trends in enthalpy and entropy of upper and lower stem melting may indicate a conformational change in the internal loop (see also below). If this is the case, it must reflect a relatively small quantitative structural change, rather than a qualitative one. The increase in $T_m$ values and free energies of melting with increasing ionic strength may influence the energetics of interaction of RNase III with its processing substrates. At physiological salt concentrations RNase III cleaves only primary sites, while at low salt secondary sites are also recognized, and otherwise unreactive RNAs are cleaved [7,10,15]. Given the salt-insensitivity of R1.1 RNA secondary structure, our results suggest that secondary site cleavage by RNase III results from an altered enzyme-substrate interaction, rather than from a salt-induced change in RNA conformation.

The R1.1 tetraloop, which is distant from the RNase III cleavage site and irrelevant to recognition [15], appears similar in conformation to a tetraloop with the same loop sequence and closing base pair [31]. The $G_{19}$ imino proton of the R1.1 tetraloop exchanges slowly with solvent, as was observed with the corresponding guanine of the model tetraloop. The GCAA tetraloop guanine imino proton is not predicted to hydrogen-bond to another nucleotide, but it may be protected from solvent exchange by hydrogen binding to a water molecule [32]. The R1.1 tetraloop is cleaved by RNase T2 at $G_{19}$, $C_{20}$, $A_{21} > C_{18} > U_{17}$, and $A_{21}$ and $A_{22}$ are the most DEPC-reactive residues. Although the NMR analysis suggests that these adenines (and in particular the N6 protons) are part of a network of hydrogen bonds, these bonds have small free energies of formation [32], and would not be expected to significantly affect the chemical or enzymatic modification reactions.

### The R1.1 internal loop

The R1.1 internal loop is asymmetric, and cannot be a canonical double helix. A lack of a rigid helical structure for this local

structure is suggested by (i) the RNase T2 sensitivity of the 3′ end-proximal portion of the internal loop, (ii) the DEPC-sensitivity of nucleotides within the internal loop, (iii) the absence of measurable protection of several of the four imino protons in the internal loop from exchange with solvent and (iv) the separate melting transitions of the upper and lower stems. The exchange-broadening of the imino protons in the internal loop and the lower stem is also evidence of flexibility. This flexibility may be responsible for the UV light-induced covalent crosslinking of the two RNase T1-resistant oligonucleotides which encompass the R1.1 internal loop [33]. The UV reactivity pattern may suggest the presence of interstrand base-stacking in the R1.1 internal loop, which occurs in 5S RNA loop E, and is responsible for the UV sensitivity of this structure [34, 35].

However, RNase III efficiently cleaves Watson–Crick base-paired dsRNA [5], so one might expect the internal loop to possess dsRNA character. Indeed, RNase V1 cleavage of the $U_{35}-G_{36}$ phosphodiester bond (which is also the primary RNase III processing site) indicates that this portion of the R1.1 internal loop is engaged in (or has access to) a helical conformation. A similar coincidence of RNase V1 and RNase III cleavage sites has also been observed in an RNase III processing signal of phage λ [36]. The unexceptional methylation sensitivity of the N7 atom of $G_{36}$ suggests that this residue is not solvent exposed. This can be contrasted with the strong chemical reactivity of the conserved guanine in the 5S rRNA internal loop E [37].

Similar internal loops are present in a number of other T7 and T3 RNase III processing signals [5,6]. Apparently this motif was selected to optimize efficient single cleavage of the phage transcripts *in vivo*. Other types of asymmetric internal loops in unrelated phage and cellular substrates also enforce single enzymatic cleavage [5,6]. It remains to be determined how processing signals with internal loops of different sequences and structures interact with RNase III to yield a similar outcome.

### The effect of magnesium

Magnesium is absolutely required for RNase III processing, so its influence on substrate structure is of particular interest. The chemical and enzymatic reactivity of R1.1 RNA is largely insensitive to magnesium, but magnesium does shift the resonances of a number of unassigned imino protons, several of which are within the internal loop, and it also affects the imino proton of the $A_9$:$U_{32}$ pair. It does not so affect the imino protons in the upper stem or tetraloop, so its effect has some specificity. The spectroscopic changes are unlikely to reflect a major conformational change in the internal loop, however, as magnesium only perturbs these resonances, instead of abolishing them or creating new ones (as seen, for example, in the binding of argininamide to the bulge loop of TAR RNA [38]). Unfortunately, no further structural information could be gained, as no NOEs between any of these resonances were detected.

Although perhaps not relevant to every processing signal, magnesium may stabilize RNA tertiary structure important for RNAse III reactivity, in addition to being an essential cofactor in the chemical step. In this regard, we have found that the interaction of R1.1 RNA with a catalytically inactive mutant of RNase III is significantly stabilized in the presence of magnesium (H.Li and A.W.N., unpublished experiments). Magnesium may therefore play an important role in the determining the reactivity of other RNase III substrates containing higher-order structural features.

### Comparison with the thermodynamically predicted secondary structure

The RNA structure prediction program MFOLD [39] predicts a lowest-energy secondary structure for R1.1[LSΔ6] RNA similar to that presented here, but with $U_7-A_9$ base-paired to $U_{35}-A_{37}$. This structure is incompatible with our assignment of imino resonance D to the $A_9$:$U_{32}$ base pair. Moreover, the computer-predicted conformation has bases $U_{32}-A_{34}$ in a bulge loop, which would coincide with several RNase V1 cleavage sites. The lowest-energy structure which contains the full-length upper stem has a similar bulge loop, but the next higher-energy structure pairs $C_6$ with $G_{36}$, and has no completely unopposed bulge loops. This internal loop pairing scheme is supported by the unexceptional DMS reactivity of $G_{36}$. This R1.1[LSΔ6] RNA structure differs from the lowest-energy conformation by less than 3 kcal/mol, which is insignificant since MFOLD neglects most non Watson–Crick interactions other than G:U base pairs, and uses thermodynamic data collected in ionic conditions (1 M NaCl) different from those used here.

For the same reason, we can only compare in a qualitative fashion our thermodynamic parameters with those calculated by MFOLD. The parameters calculated for what we argue is the most likely secondary structure of R1.1 RNA are very similar to those we observed in either salt condition (data not shown). We would expect the melting temperature to rise at higher ionic strength, but fall if additional stabilizing non Watson–Crick interactions were neglected, and perhaps the two effects cancel.

### The dsRNA mimicry model

Finally, the NMR and structure probing data presented here, as well as a previous mutational analysis [10], argue against the proposal of a more complicated internal loop folding motif [40]. Specifically, if the 'dsRNA mimicry' tertiary folding were present, we would expect an imino proton resonance from the proposed $A_5$:$U_{33}$ pair, with accompanying NOEs to adjacent base-pairs in the upper and lower stem, and these were not observed.

## CONCLUSIONS

The T7 R1.1 RNase III processing signal consists of two dsRNA stems, separated by an internal loop having a helical but relatively loosely structured conformation.

The conformation of the R1.1 processing signal is largely insensitive to the monovalent salt concentration, suggesting that secondary site versus primary site enzymatic cleavage of this substrate (and others) reflects an alteration in the enzyme-substrate complex, rather than a change in RNA conformation.

Magnesium appears to influence the structure of the internal loop. In addition to serving as the catalytic cofactor, magnesium may stabilize the proper substrate conformation for RNase III processing reactivity.

## ACKNOWLEDGEMENTS

We thank H.Li for providing purified T7 RNA polymerase and RNase III, and D.M.Crothers for the use of the UV spectrophotometer. This work was supported by NIH Grant GM41283 (to A.W.N.) and GM41651 (to P.B.M.). D.C.S. is the recipient of a Howard Hughes Medical Institute predoctoral fellowship.

## REFERENCES


1. St Johnston, D., Brown, N.H., Gall, J.G. and Jantsch, M. (1992) *Proc. Natl. Acad. Sci USA* **89**, 10979–10983.
2. Haines, D.S., Strauss, K.I. and Gillepsie, D.H. (1991) *J. Cell. Biochem.* **46**, 9–20.
3. Libonati, M., Carsana, A. and Furia, A. (1980) *Mol. Cell. Biochem.* **31**, 147–164.
4. Robertson, H.D., Webster, R.E. and Zinder, N.D. (1968) *J. Biol. Chem.* **243**, 82–91.
5. Court, D. (1993) in *Control of messenger RNA Stability* (Belasco, J. G., and Brawerman, G., eds) Academic Press, NY.
6. Dunn, J.J. and Studier, F.W. (1983) *J. Mol. Biol.* **166**, 477–535.
7. Dunn, J.J. (1976) *J. Biol. Chem.* **251**, 3807–3814.
8. Saito, H. and Richardson, C.C. (1981) *Cell* **27**, 533–542.
9. Nicholson, A.W., Niebling, K.R., McOsker, P.L. and Robertson, H.D. (1988)*Nucleic Acids Res.* **46**, 1577–1591.
10. Chelladurai, B.S., Li, H. and Nicholson, A.W. (1991) *Nucleic Acids Res.* **19**, 1759–1766.
11. Panayotatos, N. and Truong, K. (1985) *Nucleic Acids Res.* **13**, 2227–2240.
12. Linn, T. and St. Pierre, R. (1990) *J. Bacteriol.* **172**, 1077–1084.
13. Studier, F.W., Rosenberg, A.H., Dunn, J.J. and Dubendorff, J.W. (1990) *Methods Enzymol.* **185**, 60–89.
14. Ziemke, P. and McCarthy, J.E.G. (1992) *Biochim. Biophys. Acta* **1130**, 297–306.
15. Chelladurai, B.S., Li, H., Zhang, K. and Nicholson, A.W. (1993) *Biochemistry* **32**, 7549–7558.
16. Grodberg, J. and Dunn, J.J. (1988) *J. Bacteriol.* **170**, 1245–1253.
17. Li, H., Chelladurai, B.S., Zhang, K. and Nicholson, A.W. (1993) *Nucleic Acids Res.* **21**, 1919–1925.
18. Milligan, J.F., Groebe, D.R., Witherell, G.W. and Uhlenbeck, O.C. (1987) *Nucleic Acids Res.* **15**, 8783–8798.
19. Wyatt, J.R., Chastain, M. and Puglisi, J. D. (1991) *Biotechniques* **11**, 764–769.
20. Kime, M.J. and Moore, P.B. (1983) *FEBS Lett.* **153**, 199–203.
21. Kime, M.J. and Moore, P.B. (1983) *Biochemistry* **22**, 2615–2622.
22. Takegoshi, K., Tsuda, S. and Hikichi, K. (1990) *J. Mag. Res.* **89**, 399–405.
23. 'fit', J. Tirado-Rives, Dept. of Chemistry, Yale University.
24. Ehresmann, C., Baudin, F., Mougel, M., Romby, P., Ebel, J-P. and Ehresmann, B. (1987) *Nucleic Acids Res.* **15**, 9109–9128.
25. Peattie, D.A. and Gilbert, W. (1980) *Proc. Natl. Acad. Sci. USA* **77**, 4679–4682.
26. Szewczak, A.A., White, S.A., Gewirth, D.T. and Moore, P.B. (1990) *Nucleic Acids Res.* **18**, 4139–4142.
27. Searle, M.S. and Williams, D.H. (1993) *Nucleic Acids Res.* **21**, 2051–2056.
28. Lowman, H.B. and Draper, D.E. (1986) *J. Biol. Chem.* **261**, 5396–5403.
29. Lockard, R.E. and Kumar, A. (1981) *Nucleic Acids Res.* **9**, 5125–5140.
30. Auron, P.E., Weber, L.D. and Rich, A. (1982) *Biochemistry* **21**, 4700–4706.
31. Heus, H.A. and Pardi, A. (1991) *Science* **253**, 191–194.
32. SantaLucia, J., Kierzek, R. and Turner, D.H. (1992) *Science* **256**, 217–219.
33. Robertson, H.D. (1990) *Methods Enzymol.* **181**, 189–202.
34. Branch, A.D., Benenfeld, B.J., and Robertson, H.D. (1985) *Proc. Natl. Acad. Sci USA* **82**, 6590–6594.
35. Wimberly, B., Varani, G., and Tinoco, I. (1993) *Biochemistry* **32**, 1078–1087.
36. Steege, D.A., Cone, K.C., Queen, C. and Rosenberg, M. (1987) *J. Biol. Chem.* **262**, 17651–17658.
37. Romaniuk, P.J. , deStevenson, I.L., Ehresmann, C., Romby, P., and Ehresmann, B. (1988) *Nucleic Acids Res.* **16**, 2295–2312.
38. Puglisi, J.D., Tan, R., Culman, B.J., Frankel, A.D. and Williamson, J.R. (1992) *Science* **257**, 76–80.
39. Zuker, M. (1989) *Science* **244**, 48–52.
40. Robertson, H.D. and Barany, F. (1978) in *Proceedings of the 12th FEBS Congress*, Pergamon Press, NY pp. 285–295.